

Electronic Supplementary Information

New aspect of photophysics of 7,7,8,8-tetracyanoquinodimethane and its solvated complexes: intra- vs inter-molecular charge-transfer

Satoru Muramatsu,^a Nobumasa Chaki,^a Shin-nosuke Kinoshita,^a

Yoshiya Inokuchi,^a Manabu Abe,^a Toshifumi Iimori,^b and Takayuki Ebata^{a,c,d*}

^aDepartment of Chemistry, Graduate School of Advanced Science and Engineering, Hiroshima University, 1-3-1 Kagamiyama, Higashi-Hiroshima-shi, Hiroshima 739-8526, Japan

^bDepartment of Sciences and Informatics, Muroran Institute of Technology, 27-1 Mizumoto-cho, Muroran, Hokkaido 050-8585, Japan.

^cDepartment of Applied Chemistry and Institute for Molecular Science, National Chiao Tung University, Hsinchu 30010, Taiwan

^dDepartment of Applied Chemistry and Institute for Molecular Science, National Yang Ming Chiao Tung University, Hsinchu 30010, Taiwan

E-mail: tebata@nctu.edu.tw

Contents:

Figure S1. Comparison of LIF excitation spectra of TCNQ at 23800–29000 cm^{-1} region recorded by OPO laser (resolution: $\sim 7 \text{ cm}^{-1}$) and dye laser ($\sim 0.2 \text{ cm}^{-1}$).

Figure S2. ^1H NMR charts of the TCNQ sample before and after the LIF spectroscopic experiment.

Figure S3. LIF excitation spectrum of TCNQ (identical to Figure 1a in the manuscript), and fluorescence decay curve of the vibronic bands.

Figure S4. Vertical energy level diagram of S_n ($n = 1-7$) states with respect to S_0 calculated at CAM-B3LYP/6-311++G(d,p) level.

Figure S5. Binding energy and structural details of higher energy isomers of TCNQ-ACN complex.

Figure S6. LIF excitation spectrum of TCNQ with and without mixing of benzene vapor in a carrier gas.

Figure S7. Binding energy and structural details of higher energy isomers of TCNQ-benzene complex.

Figure S8. Logarithmic plots of fluorescence decay curves of TCNQ in pure benzene solvents (detection wavelength: 630 nm).

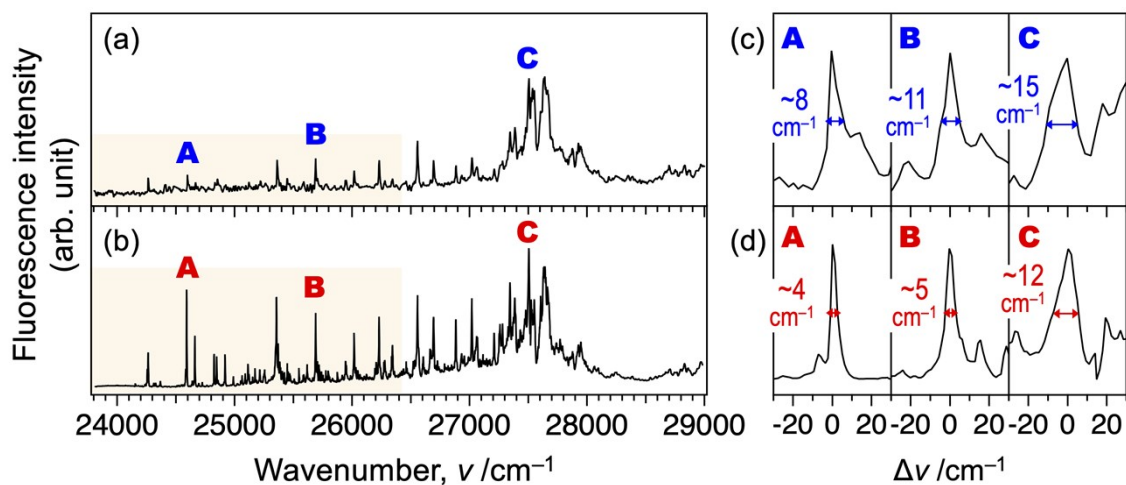


Figure S1. Comparison of LIF excitation spectra of TCNQ at 23800–29000 cm^{-1} region recorded by (a) OPO laser (resolution: $\sim 7 \text{ cm}^{-1}$) and (b) dye laser ($\sim 0.2 \text{ cm}^{-1}$), where the band intensity is normalized by laser fluence. The intensity at low wavenumber region ($< \sim 26400 \text{ cm}^{-1}$; highlighted in orange) seems different. (c and d) Expanded views of the bands **A**, **B**, and **C** in the panels (a) and (b), respectively. The FWHM values are shown to demonstrate the difference of the band widths. Panel (a) is reproduced from Ref. 20 in the manuscript with permission. Panel (b) is identical to Figure 1a in the manuscript.

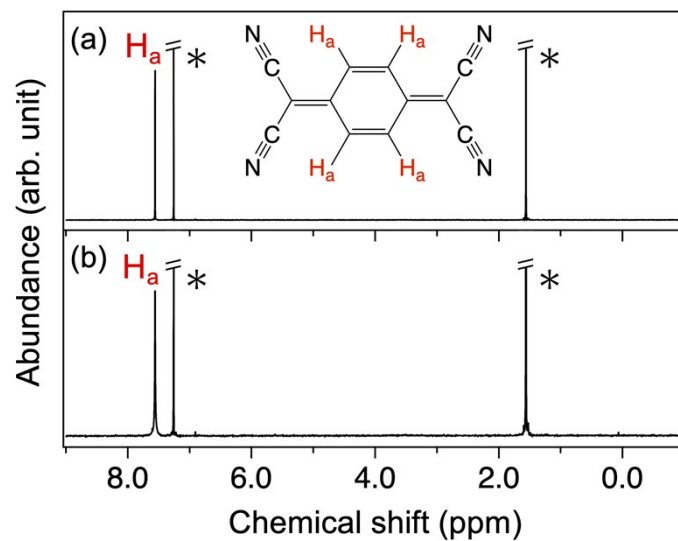


Figure S2. ^1H NMR charts of the TCNQ sample (a) before and (b) after the LIF spectroscopic experiment (300 MHz, room temperature, solvent: CD_2Cl_2). The singlet peak at 7.56 ppm is assigned to the H_a proton as shown in the inset, while peaks with asterisks are derived from the solvent (7.26 ppm) and water impurities (1.56 ppm).

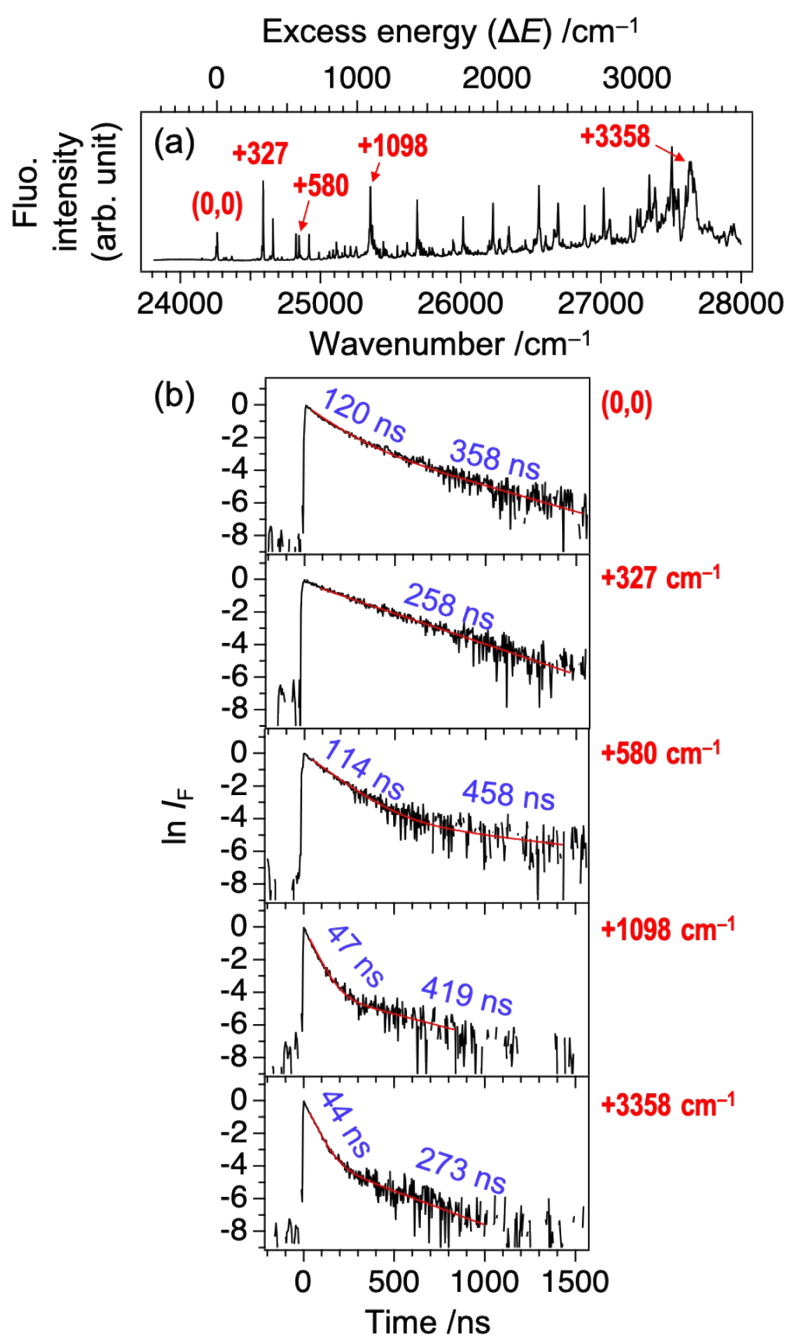


Figure S3. (a) LIF excitation spectrum of TCNQ (identical to Figure 1a in the manuscript). (b) Fluorescence decay curve of the vibronic bands with excess energy of 0 (“0,0”), +327, +580, +1098, and +3358 cm^{-1} (see Panel (a)). The curves are shown in logarithmic scale after normalization at $t = 0$, to clearly indicate the double decay feature at (0,0), +580, +1098, and +3358 cm^{-1} bands.

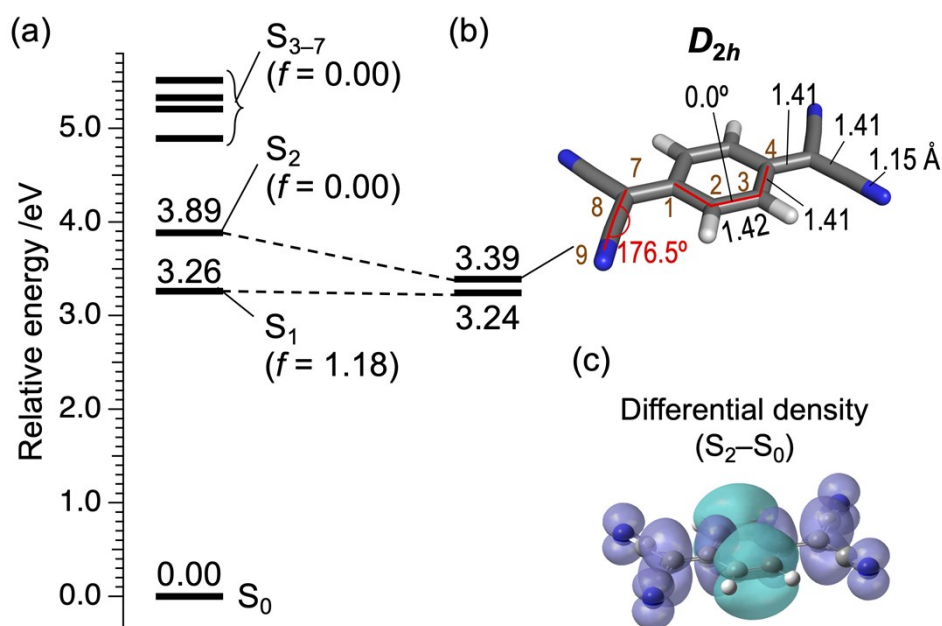


Figure S4 (a) Vertical energy level diagram of S_n ($n = 1-7$) states with respect to S_0 calculated at CAM-B3LYP/6-311++G(d,p) level. Calculated oscillator strength (f) is shown in parentheses. (b) Energy level of S_1 and S_2 at local minimum structure of S_2 , and its structural details. Bond lengths and angles are shown in angström (Å) and degrees ($^\circ$), respectively. Atom labels (1-4, 7-9) are identical to those in Chart 1b in the manuscript. Note that the C(1)-C(2)-C(3)-C(4) dihedral angle is 0.0° at this computational level while other structural parameters and energy values are almost identical to those at M06-2X/6-311++G(d,p) (see Figure 4). Color codes: grey = C, white = H, blue = N. (c) Differential density surface between S_2 and S_0 states (isodensity value: 0.0004). Electrons are transferred from the cyan to violet part upon the $S_0 \rightarrow S_2$ transition.

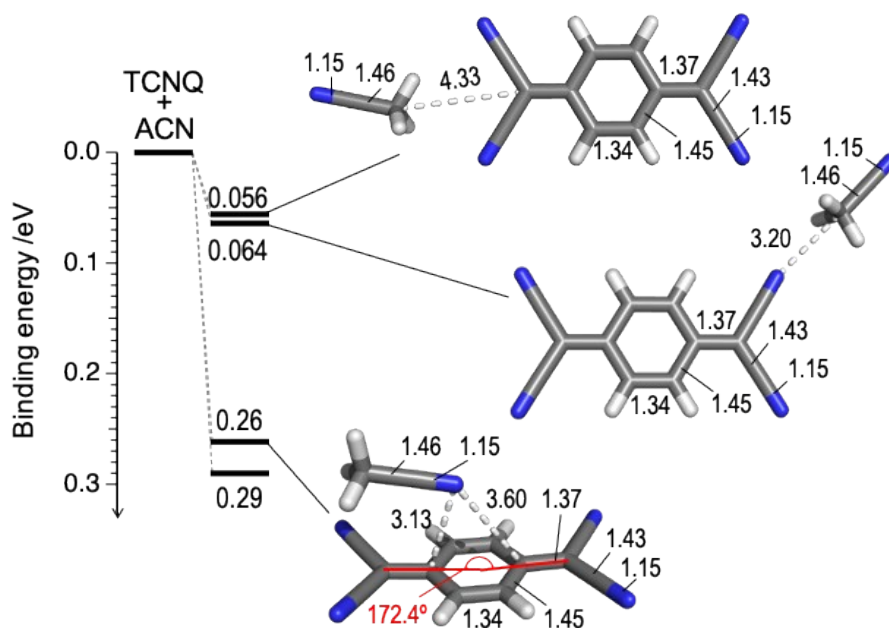


Figure S5. Binding energy and structural details of higher energy isomers of TCNQ-ACN complex. Binding energy is defined as energy difference between ACN-TCNQ complex and TCNQ + ACN at infinite distance [$E(\text{ACN-TCNQ}) - \{E(\text{TCNQ}) + E(\text{ACN})\}$]. Bond lengths and angles are shown in angström (Å) and degrees ($^{\circ}$), respectively. Color codes: gray = C, white = H, blue = N. For the structure of the most stable isomer (binding energy = 0.29 eV), see the manuscript.

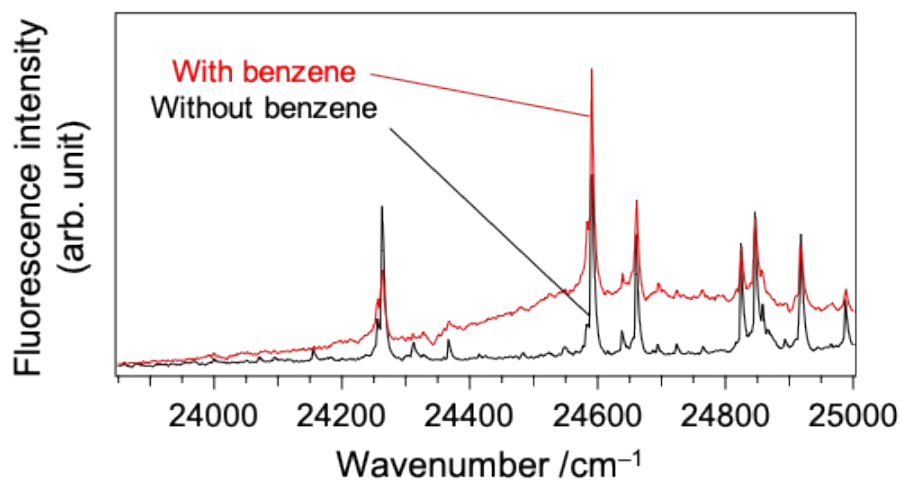


Figure S6. (a) LIF excitation spectrum of TCNQ (red) with and (black) without mixing of benzene vapor in a carrier gas. The red spectrum is identical to Figure 5a in the manuscript.

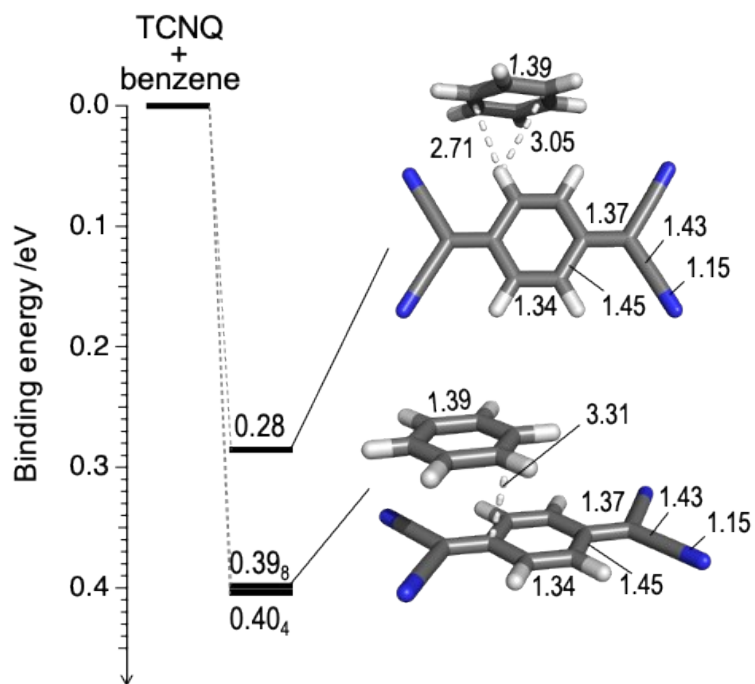


Figure S7. Binding energy and structural details of higher energy isomers of TCNQ-benzene complex. Binding energy is defined as energy difference between ACN-benzene complex and TCNQ + benzene at infinite distance [$E(\text{ACN-benzene}) - \{E(\text{TCNQ}) + E(\text{benzene})\}$]. Bond lengths are shown in angström (Å). Color codes: gray = C, white = H, blue = N. For the structure of the most stable isomer (binding energy = 0.40 eV), see the manuscript.

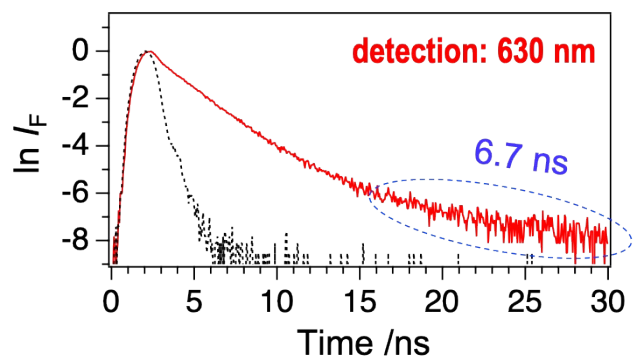


Figure S8. Logarithmic plots of fluorescence decay curves of TCNQ in pure benzene solvents (detection wavelength: 630 nm). The excitation wavelength is 390 nm. Dotted lines are background (scattered) signals. The profile exhibits multiple decay feature, although the fast components seem to include large contribution of scattered signal and to be inaccurate; it is because of quite low fluorescence intensity in pure benzene solvent due to quenching effect. We conclude that the slow component, with time constant of 6.7 ns, reflects CT emission from TCNQ-benzene complexes.